On the wafer/pad friction of linear chemical-mechanical planarization (CMP): modeling, analysis and experiments

Jingang Yi
Lam Research Corporation
CMP/Cleaning Technology Division
Fremont, CA 94538

Abstract— **In this paper we present a modeling and monitoring scheme of the friction between the wafer and polishing pad for the linear chemical-mechanical planarization (CMP) processes. Kinematic analysis of the linear CMP system is investigated and a distributed LuGre dynamic friction model is utilized to capture the friction forces generated by the wafer/pad interactions. We present an experimental validation of wafer/pad friction modeling and analysis. Pad conditioning and wafer film topography effects on the wafer/pad friction are also experimentally demonstrated. Finally one application example is illustrated the use of friction torques for real-time monitoring the shallow trench isolation (STI) CMP processes.**

I. Introduction

Chemical-mechanical planarization (CMP) is an important enabling technology in microelectronics manufacturing. During a CMP process, the wafer is pushed down against a moving polishing pad in order to achieve surface planarization. Slurry fluids are dropped on the polishing pad to assist the polishing processes. Due to the complexity of the process environments and lack of *in-situ* sensors, the CMP process is not completely understood. In recent years, various models were developed to explain the material removal mechanisms in different wafer/pad contact regimes. These contact regimes can be classified as direct contact, semi-direct contact, and lubrication and hydrodynamic contact [1], [2], [5], [6]. It has been generally considered that the thickness of the fluid thin film between wafer and pad can be used to determine which regime a particular process setup belongs to.

The characteristic of wafer/pad interface plays a very important role for the process performance. In this paper, we discuss one important mechanical aspect of such interfaces: wafer/pad friction. Direct and semi-direct contact regimes are considered in this paper between wafer and pad since it has been observed in most CMP processes [2], [6]. Sikder et al. [7] discussed measuring the coefficient of friction (COF) under various polishing parameters such as table rotating speed and polishing down force on a prototype of rotary CMP polisher without conditioning the pad. For a multi-step CMP process, polishing parameters could change within a run and therefore the friction force or torque could change. Recently, CMP processes of Cu/low-κ devices require the real-time low-friction monitoring. However, there is few research and investigation on the friction mechanism between the wafer and polishing pad and on how to monitor wafer/pad friction in real time. One of main goals of this paper is to fill such a gap. Lam linear polisher is used as an example for analysis and study. The analysis however can be extended and generalized to any other orbital and rotary CMP polishers.

The paper is organized as follows. Section II describes the Lam linear planarization technology (LPT). We also present a wafer/pad friction model with and without considering the pad conditioning effect. Friction torques applied on both spindle and roller motors are discussed. Section III discusses the effect of pattern wafer surface topography on wafer/pad friction characteristic. In section IV, experimental validations of friction model are presented. One application example of friction monitoring for shallow trench isolation (STI) device is also illustrated. Concluding remarks are presented in section V.

II. Wafer/pad Friction Model

A. Linear chemical-mechanical planarization

CMP processes use the chemical and mechanical interactions among the wafer, polishing pad, and slurry to planarize the wafer surface. In widely-used rotary CMP tools, the polishing pad is on a rotating table with a relatively large radius. The wafer carrier is rotating against the polishing pad table. The polishing pad table is normally rigid, and the wafer head carrier sometimes can be tilted or controlled by the inside air zones.

The LPT polisher uses a different mechanism. Fig. 1 shows the schematic of the Lam LPT setup. The polishing pad is moving linearly against the rotating wafer. An air-bearing supports the polishing pad from an underneath air platen. By tuning the air pressure of different air zones on the platen and adjusting platen height, we can change the polishing pad deformation and therefore control the wafer polishing uniformity in order to compensate for wafer deposition profiles. Compared with regular rotary CMP tools, the LPT design can provide a wide range of polishing

pad speed and polish pressure, and therefore increases the throughput as well as the planarization performance [8].

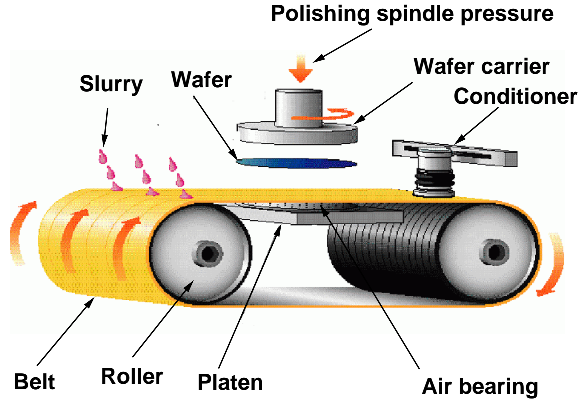

Fig. 1: Schematic of Lam linear chemical-mechanical planarization systems.

The surface of polishing pad must be maintained at a certain roughness level in order to keep the process stability. Conditioning the pad is an important and effective method for a stable process performance. In practice, a conditioning disk is pushing against on the moving polishing pad. Fig. 2 shows two different mechanisms of the pad conditioning systems: radial arm and linear conditioners.

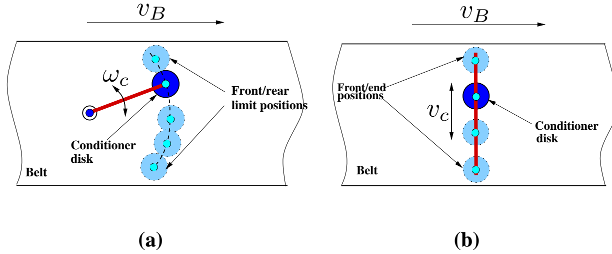

Fig. 2: LPT conditioner systems. (a) radial arm conditioner; (b) linear conditioner.

B. Friction modeling without pad conditioning

The friction force generated between the wafer and polishing pad is highly dependent on the relative velocity distribution and the pad/wafer surface characteristic. In this section, we first discuss the friction model without considering the conditioning effect and then investigate how the pad conditioning affects the friction model in the next section.

The polishing pad normally is made by a layer of polythurane. When wafer is pushed against the pad, some slurry particles are squeezed into the pad asperities and remove the wafer film during polishing. It is appropriate to consider the wafer as a rigid body. Consider the kinematic relationship of the linear CMP systems. Fig. 3 shows a schematic of a polishing wafer again the moving polishing pad. Denote the polishing pad velocity as v_B and the wafer carrier rotating speed as ω. For an arbitrary point A on the wafer surface, it is easy to calculate the relative velocity of a point A on the wafer with respect to the point on the pad that is contacted with A as

$$\mathbf{v}_{rel} = \dot{\mathbf{r}} - v_B \mathbf{i} = (-\omega r \sin\phi - v_B)\mathbf{i} + (\omega r \cos\phi)\mathbf{j}\,,$$

and the relative velocity magnitude is

$$|\mathbf{v}_{rel}| = \sqrt{\omega^2 r^2 + 2 v_B \omega r \sin\phi + v_B^2}\,, \tag{1}$$

where r is the distance from point A to the origin O, ϕ is the angle between vector $\overrightarrow{OA}$ and x axis, and $\mathbf{i}$ and $\mathbf{j}$ are the x, y unit vectors, respectively.

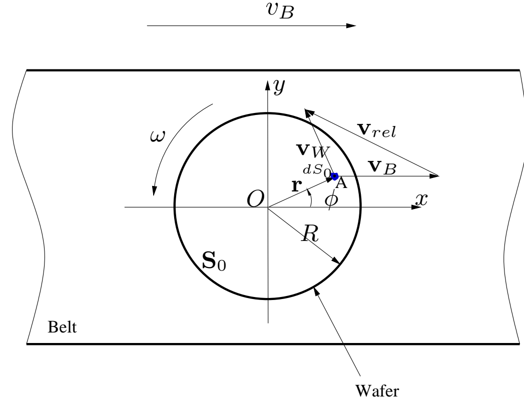

Fig. 3: A schematic of kinematic relationship of linear CMP.

Assume that the average contact pressure p_0 between the wafer surface and the pad asperities is uniformly distributed cross the wafer. Denote the whole wafer surface area S_0. Consider a small piece of area dS_0 around the point A on the wafer. Using the distributed LuGre dynamic friction model [9], we can calculate the friction force $\delta\mathbf{F}$ generated on dS_0 as

$$\begin{cases} \frac{d\delta\mathbf{z}}{dt} = \mathbf{v}_{rel} - \theta\frac{\sigma_0|\mathbf{v}_{rel}|}{g(\mathbf{v}_{rel})}\delta\mathbf{z} \\ \delta\mathbf{F} = (\sigma_0\delta\mathbf{z} + \sigma_1\delta\dot{\mathbf{z}} + \sigma_2\mathbf{v}_{rel})\,\delta F_n\,, \end{cases} \tag{2}$$

where $\delta\mathbf{z}$ is the average friction bristle deformation vector on dS_0, σ_i, $i = 0, 1, 2$, are the friction model parameters, and δF_n is the normal force applied on dS_0. The parameter θ is used to model the variations of the wafer/pad contact conditions. The function $g(\mathbf{v}_{rel})$ is given by

$$g(\mathbf{v}_{rel}) = \mu_c + (\mu_s - \mu_c)e^{-\frac{|\mathbf{v}_{rel}|}{v_s}}\,, \tag{3}$$

where μ_c and μ_s are the Coulomb and static friction coefficients between the wafer and pad surface, respectively, and v_s is the Stribeck velocity.

For the uniformly distributed pressure across the whole wafer disk, $\delta F_n = p_0$. The total friction force $\mathbf{F}$ and spindle moment $\mathbf{M}^s$ [1] with respect to the wafer center O can be calculated as

$$\mathbf{F} = \int_{S_0} \delta\mathbf{F} dS_0\,, \qquad \mathbf{M}^s = \int_{S_0} \mathbf{r}\times\delta\mathbf{F} dS_0\,. \tag{4}$$

[1] We use superscript notations to indicate and distinguish spindle and roller systems respectively.

In order to analyze the relationship between polishing parameters (such as head pressure p_0, belt speed v_B, etc.) and the friction force and moments, we need to explicitly express Eq. (4) in terms of polishing parameters.

For the friction force model (2), the dynamics of friction internal state $\delta\mathbf{z}$ are much faster than the process responses. In a very short period of time, the friction force and moments have reached their steady-state values. We can therefore calculate the steady-state frictional moments by using the quasi-static solutions of Eq. (2). Using the first-order approximation of function $g(\mathbf{v}_{rel})$,

$$g(\mathbf{v}_{rel}) \approx \mu_s - (\mu_s - \mu_c)\frac{|\mathbf{v}_{rel}|}{v_s}\,, \tag{5}$$

we can compute the friction moment

$$M^{\mathrm{s}} = \frac{p_0\mu_s}{\theta}E_1(v_B,\omega) + \frac{2}{3}\pi p_0\sigma\omega R^3\,, \tag{6}$$

where $\sigma = \sigma_2 - \frac{\mu_s-\mu_c}{v_s\theta}$, R is the wafer radius and $E_1(v_B,\omega)$ is define as the integral function of v_B and ω as follows

$$E_1 = \int_0^R\int_0^{2\pi}\frac{r(\omega r + v_B\sin\phi)}{\sqrt{\omega^2r^2 + 2v_B\omega r\sin\phi + v_B^2}}d\phi dr\,. \tag{7}$$

The friction moment applied to the roller rotating axis can be estimated through the same calculation as we discussed for the spindle axis (Fig. 1). We can estimate the roller friction moment M^{r} as follows.

$$M^{\mathrm{r}} = \frac{p_0\mu_s}{\theta}E_2(v_B,\omega) + 2\pi p_0R\sigma v_B + F_c\mu_{cond}R_r\,, \tag{8}$$

where F_c is the conditioner down force, μ_{cond} is the friction coefficient between conditioner disk and pad, and R_r is the roller radius. The integral $E_2(v_B,\omega)$ is defined as

$$E_2 = \int_0^R\int_0^{2\pi}\frac{\omega r\sin\phi + v_B}{\sqrt{\omega^2r^2 + 2v_B\omega r\sin\phi + v_B^2}}d\phi dr\,. \tag{9}$$

For most CMP processes, belt speed v_B is normally fast and wafer carrier rotating speed ω is slow. Using an approximate of $|\mathbf{v}_{rel}| \approx \omega r\sin\phi + v_B$, we then can calculate the friction torques M^{s} and M^{r} as (see Appendix for more detail)

$$M^{\mathrm{s}} = \frac{1}{3}p_0\pi R^3\omega\left(\frac{\mu_s}{\theta v_B} + 2\sigma\right) \tag{10}$$

$$M^{\mathrm{r}} = 2p_0\pi RR_r\left(\frac{\mu_s}{\theta} + \sigma v_B\right) + F_c\mu_{cond}R_r\,. \tag{11}$$

C. Pad conditioning effects on friction models

In this section, we investigate how the conditioning affects the wafer/pad friction and therefore changes the friction forces and moments during polishing processes. The conditioner disk changes the abrasive surface on the polishing pad. Without loss of generality, we only consider the linear conditioner system in Fig. 2.

For the linear pad conditioning system, the conditioned pad trajectory is much easier to analyze since the linear motions of conditioner disks are decoupled in x and y directions. We can write the velocity profile of the point C of conditioner disk center on the pad as follow

$$\begin{cases} v_{Cx}(t) = v_B \\ v_{Cy}(t) = \pm v_L\,, \end{cases} \tag{12}$$

where the velocity $v_{Cy}(t)$ in y-axis direction takes positive value v_L when the conditioner disk is moving in positive y direction. The conditioner moving across belt direction is also restricted by $-L/2 \le y_C(t) \le L/2$, where L is the disk moving distant.

In the previous discussion, the wafer/pad friction coefficients μ_s, μ_c are assumed constants when there is no pad conditioning. Under pad conditioning μ_s and μ_c are no longer kept constantly since the conditioner disk changes the wafer/pad interactions. The wafer/pad friction coefficients are different between the conditioned and unconditioned portions of the polishing pad.

In order to approximately calculate the variations of the friction moment under pad conditioning, the effect of the conditioned pad portion can be calculated as a function of the fraction of the conditioned pad area $\Delta\mathbf{S(t)}$ out of the whole wafer area (Fig. 4).

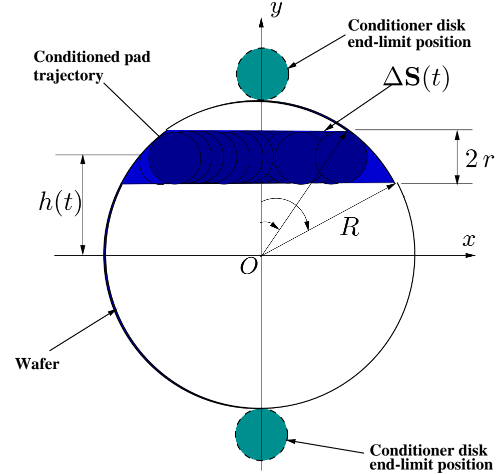

Fig. 4: A kinematic relationship between the conditioned pad portion and the wafer.

Fig. 4 shows the kinematic relationship between a conditioned pad trajectory and the polished wafer. Here we denote the conditioner disk radius as r and the distance from the wafer center to the center of the conditioner disk as $h(t)$. Denote the period of the conditioning per sweep as T_c. For simplicity, we assume that the end-limit positions of conditioner disk are tangent with the wafer surface (as shown in Fig. 4). Without loss of generality, pad conditioning is considered to move from rear to front and then back to rear (with 2 sweeps). The conditioner disk center position $h(t)$ can be calculated as

$$h(t) = \begin{cases} (R+r) - v_ct & \text{if } 0 \le t < T_c \\ -(R+r) + v_c(t - T_c) & \text{if } T_c \le t < 2T_c, \end{cases} \tag{13}$$

where v_c is the linear moving velocity of the conditioner disk.

Suppose the conditioning increases the friction coefficients (both Coulomb and static friction coefficients) by the same amount as $\gamma_\mu \geq 0$, i.e.

$$\mu_{c\text{cond}} = (1+\gamma_\mu)\mu_c\,, \quad \mu_{s\text{cond}} = (1+\gamma_\mu)\mu_s\,,$$

where $\mu_{c\text{cond}}$ and $\mu_{s\text{cond}}$ are the Coulomb and static friction coefficients with pad conditioning. We can obtain the following calculation for the spindle and roller friction torque under conditioning as a function of time $t \in [0\,, T_c)$

$$M^{\text{s}}_{\text{cond}}(t) = (1+\gamma_\mu \gamma^{\text{s}}_{\text{cond}}(t))M^{\text{s}} \tag{14}$$

$$M^{\text{r}}_{\text{cond}}(t) = (1+\gamma_\mu \gamma^{\text{r}}_{\text{cond}}(t))M^{\text{r}} + F_c \mu_c R_r\,, \tag{15}$$

where $\gamma^{\text{s}}_{\text{cond}}(t) = \frac{\Delta \mathbf{S}^{\text{s}}(t)|h(t)|}{\pi R^3}$ is the factor due to the pad conditioning at time t. In order to capture the effect of multiple pad rotating cycles, we need to modify $\Delta \mathbf{S}^{\text{s}}(t)$ in Eqs. (14) and (15) to $\Delta \mathbf{S}^{\text{s}}_e(t)$ as

$$\Delta \mathbf{S}^{\text{s}}_e(t) = \Delta \mathbf{S}^{\text{s}}(t) + \sum_{i=1}^{N} \beta_i \Delta \mathbf{S}^{\text{s}}(t - iT_B)\,, \tag{16}$$

where $0 < \beta_i < 1$, $i = 1, \ldots, N$, are the forgetting factors, and N is the number of pad rotating cycles within one conditioning sweep, $1 \leq N \leq \left[\frac{v_B T_c}{L_B}\right]$ [2]. Time constant T_B is defined as the time period for conditioned trajectory travels one belt length, i.e. $T_B = \frac{L_B}{v_B}$.

III. Pattern Wafer Topography Effect

Wafer film topography has significant impact on the wafer/pad friction and therefore on material removal rate. Due to the local wafer/pad contact pressure decrease during the polishing process, the friction force between the pattern wafer and pad also decreases. At the beginning of the pattern wafer polishing process, the local wafer/pad contact pressure $p = \delta F_n$ is not equal to the external pressure p_0 since the contact area S between wafer and pad is much smaller than the wafer disk area S_0. Assume that a pattern wafer has identical dies across the wafer and then we can obtain the average pressure δF_n as

$$\delta F_n = \frac{p_0 S_0}{S}. \tag{17}$$

Without loss of generality, in the following we discuss the shallow trench isolation (STI) device pattern wafers. Fig. 5(a) shows the schematic of the STI wafer surface cross section. Fig. 5 shows the schematic sequence of surface topography cross section changes of a STI pattern wafer during the polishing process. Let L_0 and L_A denote the pitch and active film widths respectively [3]. The pattern density ρ is defined as the ratio of trench width over the whole pitch width, i.e.

$$\rho = \frac{L_0 - L_A}{L_0} = 1 - \frac{L_A}{L_0}. \tag{18}$$

[2]The function $[x]$ means the largest integer number that is less than $x \in \mathbb{R}$.

[3]A pitch area consists of a trench and an active areas (Fig. 5(a)).

Denote the initial trench step height as h_{S0} (Fig. 5(a)). Let h_c denote the contact height at which the polishing pad starts to touch the trench oxide surface (Fig. 5(b)). In order to quantitatively model the change of the friction force during a polishing process, we consider the step height h_S decreasing model given by [10] and [11]. We consider the step height changes in two cases: $h_c \leq h_{S0}$ and $h_c > h_{S0}$.

A. **Case I:** $h_c \leq h_{S0}$

In this case, the initial step height h_{S0} is larger than the contact height h_c and the pad does not contact with the down trench oxide at the beginning of a process. The decrease of the step height $h_S(t)$ during the polishing process can be modeled as [10], [11]

$$h_S(t) = \begin{cases} h_{S0} - \frac{RR_B}{\rho} t & 0 \leq t < t_c \\ h_c e^{-\frac{t-t_c}{\tau_B}} & t \geq t_c\,, \end{cases} \tag{19}$$

where RR_B is the blanket oxide wafer removal rate, h_{S0} is the initial step height, t_c is the timing when the step height h_S reaches the contact height h_c and $\tau_B = \frac{\rho h_c}{RR_B}$ is the delaying constant.

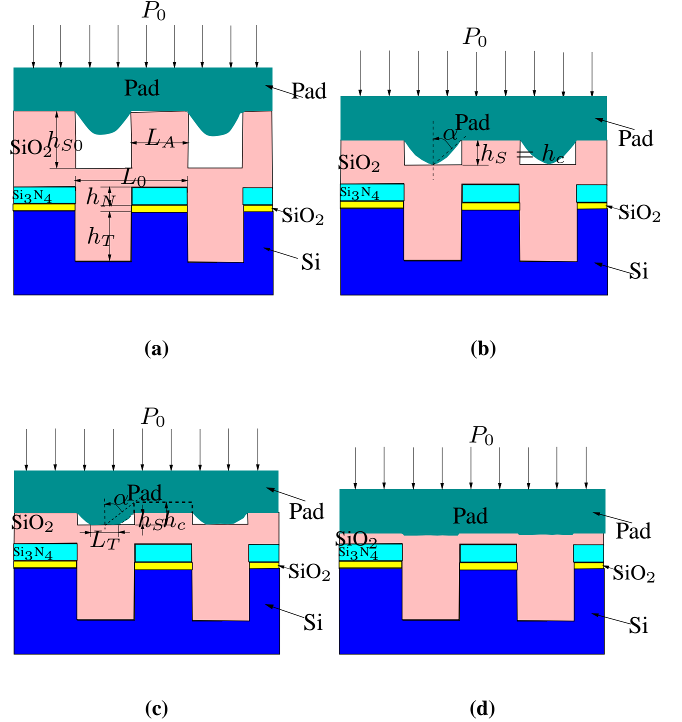

Fig. 5: A schematic snapshot of STI pattern wafer surface cross section during a polishing process, (a) starting polishing, (b) at contact height, (c) pad touchdown with trenches, (d) surface planarized.

For simplicity, all dies across the STI wafer are assumed the same density and pitch width. We then have uniformly polishing profile across the wafer. Define the pattern effect

factor $\gamma_{\text{patt}}(t)$ as

$$\gamma_{\text{patt}}(t) = \frac{S_0}{S} = \frac{S_c}{S_P} = \begin{cases} \frac{1}{1-\rho} & 0 \le t < t_c \\ \frac{1}{1-\rho e^{-\frac{t-t_c}{\tau_B}}} & t \ge t_c \,. \end{cases} \quad (20)$$

B. Case II: $h_c > h_{S0}$

In this case, the pad already contacts the down trench area when the polishing starts. Similarly we can define the pattern effect factor γ_{patt} for friction model as

$$\gamma_{\text{patt}}(t) = \frac{S_0}{S} = \frac{S_c}{S_P} = \frac{1}{1 - \frac{h_{S0}}{h_c}\rho e^{-\frac{t}{\tau_B}}} \quad (21)$$

Therefore, for pattern wafer polishing with pad conditioning, the spindle and roller motor torques can be modified as

$$M^{\text{s}}_{\text{patt}}(t) = \gamma_{\text{patt}}(t)(1 + \gamma_\mu \gamma^{\text{s}}_{\text{cond}}(t))M^{\text{s}}$$
$$M^{\text{r}}_{\text{patt}}(t) = \gamma_{\text{patt}}(t)\left[1 + \gamma_\mu \gamma^{r}_{\text{cond}}(t)\right] M^{\text{r}} + F_c \mu_{\text{cond}} R_r \,. \quad (22)$$

IV. Experimental Results

A. Model validation

Some experiments have been carried out to validate the friction models discussed in previous sections. A baseline CMP process is used to study the conditioning effect. Some other processes are compared with the baseline process by only varying one process parameter at a time, such as wafer carrier speed ω and belt speed v_B, etc. Thermal oxide wafers, Cabot SS12 slurry and Rodel IC 1000 pad are used on Lam Teres CMP polishers.

We will not go through the detail discussions of model validation. Instead, we present some comparisons between model predictions and experimental results. The friction model parameters are first estimated using some experiments and then used to predict the friction torques. For example, from some experiments we estimate $\Theta = \left[\frac{\mu_s}{\theta} \quad \sigma\right] = [0.0323 \quad -0.0085]$ and we use these parameter values in the model predictions. Fig. 6 shows the roller torques under different pad conditioning setups. Model prediction results are also plotted with the experimental data. Fig. 6(a) shows the roller torque under a process with 100 % pad conditioning and 3 lbs conditioner downforce [4]. Fig. 6(b) shows the roller torque under the same process except a 50 % pad conditioning and 7 lbs conditioner downforce. In the estimation we use $\gamma_\mu = 0.8$, $\beta_1 = 0.7$, and $\beta_2 = 0.3$. From these two examples, we can clearly see that the proposed models give accurate estimates of the roller motor torque.

B. One application example

As an application, we demonstrate one example of friction torque prediction and monitoring when polishing a shallow trench isolation (STI) test wafer.

[4]The percentage of conditioning is defined as the ratio of conditioning process time over the whole process time.

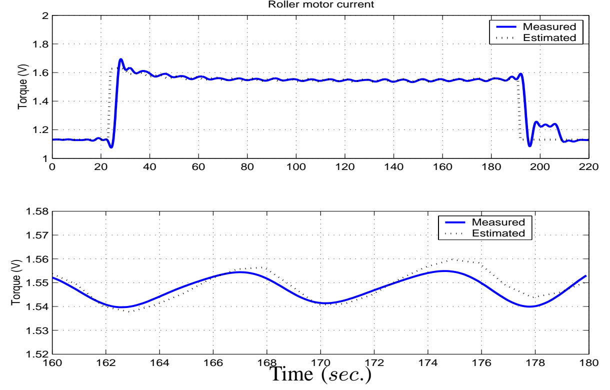

(a)

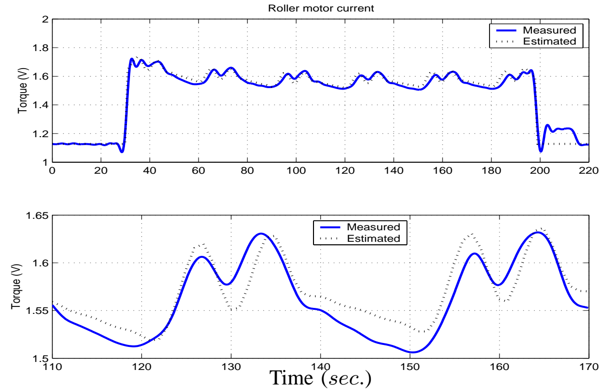

(b)

Fig. 6: An example of roller motor torques, (a) 100% conditioning with a 3 lbf conditioner down force, (b) 50% conditioning with a 7 lbf conditioner down force.

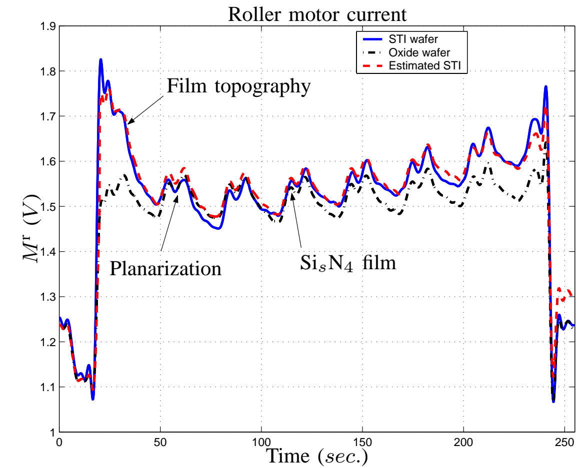

Fig. 7: Friction monitoring for a blanket and an STI wafers process.

Fig. 7 shows the roller torques of polishing STI test wafers. The CMP process recipe is the same as the previous

examples except a longer polishing time (224 *sec.*) A comparison torque for oxide monitor wafers using the same recipe is also plotted in the same figure. We can clearly notice the difference of roller motor currents between STI and oxide wafers. When we polish STI pattern wafers, the roller motor current is high at a first few seconds compared with oxide blanket wafer polishing because of variations of pattern density and film topography. When the process continues, the film surface becomes smooth and therefore the roller motor current follows the blanket oxide wafer polishing trace. The roller motor current measurement clearly demonstrates the change of the pad/wafer contact and planarization of the wafer surface. Clearly we can see a very good fit between the estimated and real friction torques. Using the estimate of the roller friction torque, we can monitor the process in real time. It is extremely useful for CMP processes since no availability of in-situ sensors to real-time monitor the processes.

V. Conclusion

In this paper, we discussed the wafer/pad friction characteristic based on the Lam linear CMP polisher. We first investigated the kinematic relationship of wafer and pad interactions and a distributed LuGre dynamic friction model was used to capture the friction characteristic. Since it is difficult to measure the wafer/pad friction directly, we proposed to use the polisher spindle and roller motor torques to monitor the friction. An analytical relationship between wafer/pad friction coefficients, polishing parameters and spindle and roller torques has been proposed. Moreover, we investigated the impact of the pad conditioning and pattern wafer topography on the wafer/pad friction. We found that the roller motor torque could be a good candidate to monitor the wafer/pad friction as well as other polishing parameters. The estimate of the spindle and roller motor torques fits the experimental measurements very well. Different experiments and processes have been designed to verify the theoretical findings and analyses. The experimental results have confirmed the proposed friction models for both oxide and STI pattern wafer processes. The proposed friction model and estimation schemes can be further investigated and applied to CMP process monitoring in future, such as process fault detection and identification.

References

[1] D. Wang, J. Lee, K. Holland, T. Bibby, S. Beaudoin, and T. Cale, "Von Mises Stress in Chemical-Mechanical Polishing Processes," *Journal of Electrochemical Society*, vol. 144, no. 3, pp. 1121–1127, 1997.

[2] G. Fu, A. Chandra, S. Guha, and G. Subhash, "A Plasticity-Based Model of Material Removal in Chemical-Mechanical Polishing (CMP)," *IEEE Trans. Semiconduct. Manufact.*, vol. 14, no. 4, pp. 406–417, 2001.

[3] S. Runnels and L. Eyman, "Tribology Analysis of Chemical-Mechanical Polishing," *Journal of Electrochemical Society*, vol. 141, no. 6, pp. 1698–1701, 1994.

[4] S. Sundararajan, D. Thakurta, D. Schwendeman, S. Murarka, and W. Gill, "Two-Dimensional Wafer-Scale Chemical Mechanical Planarization Models Based on Lubrication Theory and Mass Transport," *Journal of Electrochemical Society*, vol. 146, no. 2, pp. 761–766, 1999.

[5] D. Thakurta, C. Borst, D. Schwendeman, R. Gutmann, and W. Gill, "Pad Porosity, Compressibility and Slurry Delivery Effects in Chemical-Mechanical Planarization: Modeling and Experiments," *Thin Solid Films*, vol. 366, pp. 181–190, 2000.

[6] J. Tichy, J. Levert, L. Shan, and S. Danyluk, "Contact Mechanics and Lubrication Hydrodynamics of Chemical Mechanical Polishing," *Journal of Electrochemical Society*, vol. 146, no. 4, pp. 1523–1528, 1999.

[7] A. Sikder, F. Giglio, J. Wood, A. Kumar, and M. Anthony, "Optimization of Tribological Properties of Silicon Dioxide during the Chemical Mechanical Planarization Process," *Journal of Electronic Materials*, vol. 30, no. 12, pp. 1520–1526, 2001.

[8] A. Jensen, P. Renteln, S. Jew, C. Raeder, and P. Cheung, "Empirical-based Modeling for Control of CMP Removal Uniformity," *Solid State Technology*, vol. 44, no. 6, pp. 101–106, 2001.

[9] C. Canudas de Wit, H. Olsson, K. Åström, and P. Lischinsky, "A New Model for Control of Systems with Friction," *IEEE Trans. Automat. Contr.*, vol. 40, no. 3, pp. 419–425, 1995.

[10] T. Smith, S. Fang, D. Boning, G. Shinm, and J. Stefani, "A CMP Model Combining Density and Time Dependencies," in *Proceedings of CMP-MIC Conference*, Santa Clara, CA, 1999, pp. 97–104.

[11] B. Lee, "Modeling of Chemical Mechanical Polishing for Shallow Trench Isolation," Ph.D. dissertation, Department of Electrical Engineering and Computer Science, Massachusetts Institute of Technology, 2002.

Appendix

By approximation, the magnitude of the moment $M^{\rm s}$ is calculated as

$$M^{\rm s} = \int_0^R \frac{pr\mu_s}{\theta}\int_0^{2\pi}\frac{\omega r + v_B\sin\phi}{\omega r\sin\phi + v_B}d\phi dr + \int_0^R pr\sigma\int_0^{2\pi}(\omega r + v_B\sin\phi)d\phi dr\,. \qquad (23)$$

Define $\alpha = \frac{\omega r}{v_B}$ and we can calculate the first integral in the above equation as

$$\begin{aligned}
&\int_0^R \frac{pr\mu_s}{\theta}\int_0^{2\pi}\frac{\omega r + v_B\sin\phi}{\omega r\sin\phi + v_B}d\phi dr \\
&= \int_0^R \frac{pr\mu_s}{\theta}\int_0^{2\pi}\frac{\alpha+\sin\phi}{\alpha\sin\phi+1}d\phi dr \\
&= \int_0^R \frac{pr\mu_s}{\theta}\frac{2\pi}{\alpha}\left(1-\sqrt{1-\alpha^2}\right)d\phi dr \\
&\approx \int_0^R \frac{pr\mu_s}{\theta}\frac{2\pi}{\alpha}\left[1-\left(1-\frac{1}{2}\alpha^2\right)\right]d\phi dr \\
&= \int_0^R \frac{pr\mu_s}{\theta}\pi\alpha dr\,, \qquad (24)
\end{aligned}$$

where we use the fact $(1-\alpha^2)^{1/2} \approx 1-\frac{1}{2}\alpha^2$ since $0 < \alpha \ll 1$. Combining Eq. (24) into Eq. (23), we obtain the formula for the friction moments Eq. (10) as

$$\begin{aligned}
M^{\rm s} &= \int_0^R pr\frac{\mu_s}{\theta}\frac{\pi}{v_B}\omega r dr + \int_0^R pr\int_0^{2\pi}\sigma(\omega r + v_B\sin\phi)d\phi dr \\
&= \frac{1}{3}\pi p R^3\omega\left(\frac{\mu_s}{\theta v_B}+2\sigma\right)\,.
\end{aligned}$$